# Pressure Swing Adsorption: An Experimental Study of Diffusion-Induced Separation

Gas separation based on differences in intraparticle diffusion rates was achieved by four-step pressure swing adsorption (PSA) process. The application studied was the separation of nitrogen from air using molecular sieve type RS-10. Systematic PSA experiments were conducted in bench-scale equipment to study several variables, including duration of steps of the cycle, flow rates, pressure ratio, subatmospheric blowdown and purge, and column geometry.

The test results were compared with predictions of a mathematical model (Shin and Knaebel, 1987). In all cases, the trends of product purity and net recovery of both theory and experiment were in close agreement. Since the theory accurately portrays the overall behavior of the process, the transport mechanisms embodied in the theory may provide insight into diffusion-induced separation by PSA. In addition, by reviewing the results of the parametric studies of the variables, it has been possible to gain an intuitive understanding of the relations between factors that affect each step, and hence overall performance.

**H.-S. Shin and K. S. Knaebel**
Department of Chemical Engineering
The Ohio State University
Columbus, OH 43210

## Introduction

Pressure Swing Adsorption (PSA) has become a subject of interest for small-scale gas separation because of its potential for high separation performance (in terms of product purity and recovery), compared with alternate technologies. Depending on the mechanism that is exploited, PSA separations can be categorized as equilibrium-based or diffusion-induced. Equilibrium-based separation, which exploits the differences in equilibrium capacities of gases on an adsorbent, has been fairly well established theoretically and experimentally and already commercialized for some applications (Ruthven, 1984; Wankat, 1986; Yang, 1987). In contrast, diffusion-induced separation exploits differences in intraparticle rates of diffusion within an adsorbent. This approach has been developed over the past decade as manufacturing techniques for suitable carbon and zeolite molecular sieves have advanced. To date, only production of nitrogen from air is known to be commercialized.

Recently, several experimental studies and theoretical models of diffusion-induced separation have been published (Yang and Doong, 1985; Doong and Yang, 1986, 1987; Hassan et al. 1986, 1987). They focused primarily on presentation of the theoretical models and the effects of a few variables on performance.

The operation of the diffusion-induced PSA process is more subtle than that of the equilibrium PSA process because the concentration profile produced along a bed cannot be kept very sharp, as it is effected by differences in kinetic selectivity of gases into the adsorbent. Therefore, to gain a thorough understanding of the diffusion-induced PSA process, a systematic study of the effects of operating conditions and design variables on PSA performance is needed. The primary scope of this paper is to present bench-scale experimental data and to test our previous model (Shin and Knaebel, 1987). The system studied here is nitrogen production from air with molecular sieve RS-10. Several operating parameters (including step time, inlet velocities, pressure ratio, subatmospheric blowdown and purge, and column geometry) were examined in terms of product recovery and purity.

## Numerical Simulation

Numerical simulations were performed using the model in our previous paper (Shin and Knaebel, 1987). That model was comprised of separate continuity equations that applied within the adsorbent particles and along the bed axis. Fick's law was presumed to apply for each component within the particles, based on independent effective diffusivities. The time and position dependence of compositions, velocities, etc., was determined by orthogonal collocation and integration by Gear's method.

Actually, this model is not likely to depict the concentration profiles within an adsorbent particle *per se,* because there exists a bidisperse pore size distribution and the limiting diffusion

Correspondence concerning this paper should be addressed to K. S. Knaebel.

resistance is likely within the micropores of the 1- to 10-$\mu$m-sized crystals. If that is true, the size of a crystal may be scaled to that of a particle and the predicted concentration profiles may be considered to be those within a crystal, while the composition profiles within the macropores of a particle remain essentially flat.

All the required parameters in the simulations were measured in separate experiments except for the effective diffusivity of oxygen and the diffusivity ratio of nitrogen and oxygen. Since diffusivities of gases in porous solids are known to depend on pressure and temperature and those, along with the external film composition and the intraparticle concentration profiles, vary significantly during the PSA cycle, it was felt that classical techniques for measuring diffusivities would not have clear correspondence to actual PSA operation. Consequently, those two diffusivity parameters were estimated by simulating the PSA process over a range of operating conditions for a series of trial values and comparing the results with experimental counterparts. Specifically, the experiments analyzed in this manner were 1–4, 13–15, and 20–23 (cf. Table 1). Subsequently, PSA performance was predicted for other operating conditions, adjusting no parameters. This approach may have partially compensated for inadequacies of the model, i.e., by empirically and implicitly accounting for effects that were not explicitly dealt with in the model.

A large-film mass-transfer coefficient was used because for all cases empirical estimates implied that film mass transfer resistance was negligible compared to intraparticle mass trans-

**Table 1. Experimental Conditions and Corresponding Experimental and Theoretical Results**

| Expt. No. | Duration $t_1$ | $t_2$ | $t_3$ | $t_4$ | High Pres. (kPa) | Low Pres. (kPa) | Temp. (°C) | Blowdown & Purge* | Column Type** | $N_H \times 10^3$ ($m^3$ at STP) | $N_{Pu} \times 10^3$ ($m^3$ at STP) | % Recovery Exp. | % Recovery Theory | $N_2$ mol % Exp. | $N_2$ mol % Theory |
|---|---|---|---|---|---|---|---|---|---|---|---|---|---|---|---|
| 1 | 25 | 2 | 3 | 15 | 358 | 117 | 23.5 | A | I | 0.182 | 0.0166 | 6.44 | 6.38 | 99.75 | 100.0 |
| 2 | 30 | 2 | 3 | 15 | 358 | 118 | 22.0 | A | I | 0.218 | 0.0166 | 8.16 | 8.64 | 99.55 | 99.89 |
| 3 | 35 | 2 | 3 | 15 | 358 | 117 | 23.0 | A | I | 0.254 | 0.0166 | 10.65 | 10.92 | 99.0 | 99.09 |
| 4 | 40 | 2 | 3 | 15 | 358 | 116 | 23.5 | A | I | 0.291 | 0.0166 | 12.39 | 12.15 | 98.35 | 98.59 |
| 5 | 35 | 2 | 3 | 15 | 358 | 117 | 24.5 | A | I | 0.218 | 0.0166 | 7.07 | 8.25 | 99.6 | 99.88 |
| 6 | 35 | 2 | 3 | 15 | 358 | 117 | 24.5 | A | I | 0.254 | 0.0166 | 9.41 | 9.85 | 98.85 | 99.41 |
| 7 | 35 | 2 | 3 | 15 | 358 | 116 | 25.5 | A | I | 0.273 | 0.0166 | 11.67 | 11.72 | 98.3 | 98.77 |
| 8 | 35 | 2 | 3 | 15 | 358 | 117 | 25.0 | A | I | 0.291 | 0.0166 | 12.99 | 12.13 | 97.8 | 98.49 |
| 9 | 35 | 2 | 3 | 15 | 358 | 119 | 23.0 | A | I | 0.393 | 0.0166 | 25.84 | 17.02 | 90.8 | 95.39 |
| 10 | 50 | 2 | 3 | 15 | 358 | 119 | 22.0 | A | I | 0.393 | 0.0166 | 21.36 | 16.09 | 90.7 | 96.23 |
| 11 | 70 | 2 | 3 | 15 | 358 | 118 | 22.0 | A | I | 0.393 | 0.0166 | 22.74 | 15.50 | 91.4 | 96.18 |
| 12 | 100 | 2 | 3 | 15 | 358 | 119 | 21.2 | A | I | 0.393 | 0.0166 | 22.18 | 15.96 | 91.2 | 96.02 |
| 13 | 35 | 6 | 3 | 15 | 358 | 110 | 24.0 | A | I | 0.291 | 0.0166 | 9.39 | 8.35 | 98.25 | 99.7 |
| 14 | 35 | 10 | 3 | 15 | 358 | 109 | 24.0 | A | I | 0.291 | 0.0166 | 7.40 | 6.32 | 98.9 | 99.82 |
| 15 | 35 | 15 | 3 | 15 | 358 | 107 | 25.5 | A | I | 0.291 | 0.0166 | 5.10 | 5.00 | 99.0 | 99.88 |
| 16 | 35 | 6 | 3 | 15 | 358 | 109 | 25.0 | A | I | 0.291 | 0.0166 | 9.19 | 8.59 | 98.45 | 99.63 |
| 17 | 35 | 6 | 3 | 15 | 358 | 110 | 27.0 | A | I | 0.291 | 0.0309 | 7.07 | 7.62 | 98.5 | 99.76 |
| 18 | 35 | 6 | 3 | 15 | 358 | 111 | 26.0 | A | I | 0.291 | 0.0439 | 6.43 | 6.99 | 98.7 | 99.83 |
| 19 | 35 | 6 | 3 | 15 | 358 | 111 | 25.5 | A | I | 0.291 | 0.0602 | 5.41 | 6.13 | 98.8 | 99.93 |
| 20 | 35 | 2 | 3 | 15 | 358 | 112 | 25.5 | A | I | 0.291 | 0.0166 | 11.51 | 12.44 | 97.95 | 98.71 |
| 21 | 35 | 2 | 5 | 15 | 358 | 110 | 25.0 | A | I | 0.291 | 0.0276 | 9.72 | 9.67 | 98.5 | 99.42 |
| 22 | 35 | 2 | 8 | 15 | 358 | 108 | 24.2 | A | I | 0.291 | 0.0442 | 6.74 | 6.59 | 98.85 | 99.79 |
| 23 | 35 | 2 | 11 | 15 | 358 | 107 | 24.0 | A | I | 0.291 | 0.0607 | 3.37 | 4.08 | 99.0 | 99.96 |
| 24 | 35 | 2 | 2 | 15 | 358 | 115 | 24.8 | A | I | 0.349 | 0.0439 | 16.63 | 14.33 | 95.85 | 97.47 |
| 25 | 35 | 2 | 5 | 15 | 358 | 109 | 25.8 | A | I | 0.349 | 0.0439 | 10.76 | 11.55 | 96.8 | 98.72 |
| 26 | 35 | 2 | 9 | 15 | 358 | 106 | 26.3 | A | I | 0.349 | 0.0439 | 8.57 | 8.47 | 97.3 | 99.15 |
| 27 | 35 | 2 | 12 | 15 | 358 | 105 | 24.8 | A | I | 0.349 | 0.0439 | 8.26 | 7.21 | 97.65 | 99.1 |
| 28 | 35 | 2 | 3 | 11 | 358 | 112 | 26.7 | A | I | 0.291 | 0.0166 | 7.35 | 8.56 | 98.75 | 99.87 |
| 29 | 35 | 2 | 3 | 20 | 358 | 110 | 25.2 | A | I | 0.291 | 0.0166 | 11.95 | 14.27 | 97.7 | 97.92 |
| 30 | 35 | 2 | 3 | 25 | 358 | 113 | 23.6 | A | I | 0.291 | 0.0166 | 13.30 | 16.07 | 97.0 | 96.57 |
| 31 | 35 | 2 | 3 | 15 | 200 | 113 | 22.3 | A | I | 0.393 | 0.0166 | 41.56 | 37.64 | 82.3 | 82.27 |
| 32 | 35 | 2 | 3 | 15 | 358 | 123 | 23.0 | A | I | 0.393 | 0.0166 | 22.46 | 16.07 | 93.7 | 94.97 |
| 33 | 35 | 2 | 3 | 15 | 620 | 154 | 24.5 | A | I | 0.393 | 0.0166 | 12.54 | 8.00 | 98.2 | 100.0 |
| 34 | 35 | 2 | 3 | 15 | 200 | 113 | 22.3 | A | I | 0.131 | 0.0166 | 13.83 | 13.09 | 93.8 | 94.45 |
| 35 | 35 | 2 | 3 | 15 | 620 | 152 | 25.4 | A | I | 0.663 | 0.0166 | 23.05 | 16.73 | 93.7 | 97.58 |
| 36 | 35 | 2 | 3 | 15 | 200 | 60 | 22.8 | S | I | 0.393 | 0.0166 | 28.89 | 27.70 | 86.15 | 87.93 |
| 37 | 35 | 2 | 3 | 15 | 358 | 79 | 22.5 | S | I | 0.393 | 0.0166 | 19.05 | 14.43 | 95.05 | 97.29 |
| 38 | 35 | 2 | 3 | 15 | 620 | 122 | 21.6 | S | I | 0.393 | 0.0166 | 12.03 | 7.15 | 98.4 | 100.0 |
| 39 | 35 | 2 | 3 | 15 | 200 | 60 | 22.0 | S | I | 0.218 | 0.0166 | 16.87 | 16.08 | 93.8 | 95.41 |
| 40 | 35 | 2 | 3 | 15 | 358 | 78 | 22.0 | S | I | 0.433 | 0.0166 | 21.83 | 16.06 | 93.7 | 96.24 |
| 41 | 35 | 2 | 3 | 15 | 620 | 119 | 21.5 | S | I | 0.628 | 0.0166 | 23.12 | 15.04 | 93.7 | 98.53 |
| 42 | 35 | 2 | 3 | 15 | 358 | 120 | 24.0 | A | II | 0.393 | 0.0166 | 22.40 | 16.46 | 89.0 | 94.44 |
| 43 | 35 | 2 | 3 | 15 | 358 | 125 | 24.5 | A | III | 0.393 | 0.0166 | 22.37 | 16.15 | 82.3 | 89.72 |

*Note:* Pairs of experiments like 3 and 6, 8 and 20, 9 and 32, and 13 and 16 were done under the same experimental conditions, respectively; however, the theoretical results were not same due to the variation of column low pressure and ambient temperature, which were used to calculate the interstitial velocities for simulations.

*A-atmospheric, i.e., 117.0 ± 12.0 kPa except for experiment 33; S-subatmospheric, the receiver was maintained at about 20.0 kPa, but the column pressure sometimes was as high as 122.0 kPa due to the inability of the system to accommodate large volumetric flows.

**I: $d$ = 0.0208 m, $L$ = 1.016 m; II: $d$ = 0.0394 m, $L$ = 0.284 m; III: $d$ = 0.0635 m, $L$ = 0.109 m.

The absolute percentage deviations between theory and experiment are: for recovery, average = 2.52%, maximum = 8.82%; for purity, average = 1.81%, maximum = 7.42%.

fer resistance. Similarly, the Peclet number during high-pressure feed step was calculated from an empirical correlation (Edwards and Richardson, 1968) by the use of the interstitial inlet velocity and was considered constant during all steps.

As in the previous work, the pressure in the bed at any time was specified *a priori*. In this case, experimental data were used so that the predictions closely correspond to actual experimental conditions. It was noted, however, that simpler profiles (e.g., combining the pressurization and feed steps and blowdown and purge steps, respectively, as two exponentially damped shifts) caused insignificant deviations from the exact profiles. In addition, as before eight collocation points along the radius of an adsorbent particle and six collocation points along the axis of the bed were used in all simulations. Using a VAX 8500 minicomputer, about one CPU-hour was required to reach cyclic steady state. Fewer cycles were required to attain cyclic steady state in simulations than in the corresponding experiments because the capacitance of the product tank was ignored in the theory. In addition, the purge gas composition was taken to be that of the time-averaged product from the previous feed step. As a result, simulations of either one- or two-column systems yield identical results.

## Experimental Procedure

### *Measurement of adsorbent parameters*

The required adsorption and physical properties of molecular sieve RS-10 (Union Carbide Corp.) were measured in separate experiments, and the values are summarized in Table 2. The isotherm slopes were derived from equilibrium isotherms of the pure gases at 27°C, which were measured volumetrically, Figure 1. The equilibrium adsorption isotherms of RS-10 are very similar to those of zeolite 4A measured by Ball (1985), reflecting their similar sodium alumino silicate compositions. The diffusivity data were estimated from simulations and experiments as mentioned previously, and were assumed to be independent of pressure and concentration.

### *PSA experiments*

The PSA experiments were performed for nitrogen production from air with molecular sieve RS-10. The schematic diagram of the bench-scale process is shown in Figure 2. The adsorbent was pretreated for 24 hours at 400°C under full vacuum

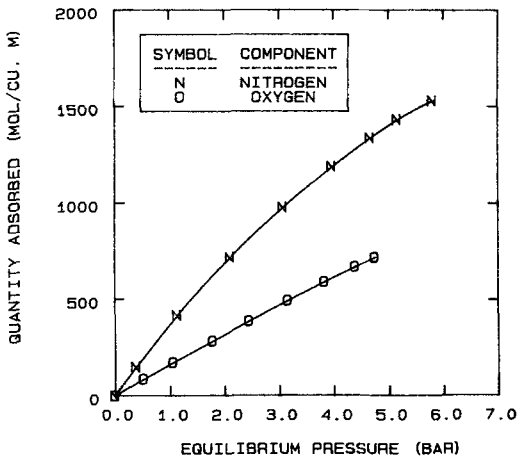


**Figure 1. Equilibrium isotherms of nitrogen and oxygen on molecular sieve RS-10 at 27°C.**

before its use. A single fixed-bed of adsorbent and a four-step PSA cycle was used to simplify control and data acquisition, and to facilitate process identification. All solenoid valves were controlled by a DEC PDP 11/73 microcomputer; and pressure, flow rates, and product concentration were acquired and simultaneously monitored on a CRT screen. When cyclic steady state was reached, the computer stored all necessary data in its virtual memory for subsequent retrieval and off-line analysis. Cyclic steady state was presumed when there were no changes in the pressure and composition in the product tank. A series of four 35-L tanks were used to minimize pressure fluctuations of the feed. In addition, a pressure controller on the feed tank helped keep the flow rate during high-pressure feed step constant.

The concentration of the product was analyzed by a Perkin-Elmer MGA-1200 Multiple Gas Analyzer. Since argon was partially isolated with nitrogen and its concentration was relatively low (less than 2%), argon was considered as a part of the nitrogen, and so air was considered to be a binary mixture. Normally, the pressurized bed after a high-pressure feed step was discharged to atmospheric pressure during blowdown and purge, except for a series of experiments employing vacuum for blowdown and purge. For those cases, the pressurized bed was discharged to the partially evacuated by-product tank.

**Table 2. Characteristics of Adsorbent and Packed Bed**

| | | | |
|---|---|---|---|
| Particle density | 1790. kg/m$^3$ | | |
| Bulk density | 724. kg/m$^3$ | | |
| Particle radius | $8 \times 10^{-4}$ m | | |
| Bed void fraction | 0.6 | | |
| Bed inner diameter | 0.0208 m | 0.0394 m* | 0.0635 m* |
| Bed length | 1.016 m | 0.284 m* | 0.109 m* |
| Effective diffusivity of $O_2$ | $3 \times 10^{-7}$ m$^2$/s | | |
| Effective diffusivity of $N_2$ | $6 \times 10^{-9}$ m$^2$/s | | |
| Eff. diffusivity ratio of $N_2$ to $O_2$: | 0.02 | | |
| Isotherm slope of $O_2$ | $3.822\left(\frac{\text{kmol/m}^3\text{ solid}}{\text{kmol/m}^3\text{ gas}}\right)$ | | |
| Isotherm slope of $N_2$ | $8.178\left(\frac{\text{kmol/m}^3\text{ solid}}{\text{kmol/m}^3\text{ gas}}\right)$, | $6.545\left(\frac{\text{kmol/m}^3\text{ solid}}{\text{kmol/m}^3\text{ gas}}\right)$** | |
| Mass transfer coefficient of $O_2$ | 10 m/s | | |
| Mass transfer coefficient of $N_2$ | 10 m/s | | |

*These two columns were used for the study of column geometry effect.
**This value was used in the numerical simulation of the feed pressure of 620 kPa due to the deviation from linearity.

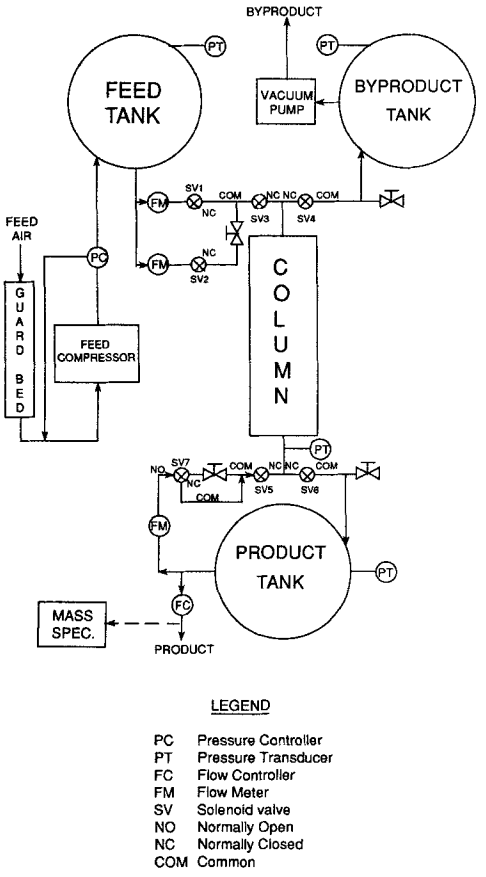


**Figure 2. PSA experimental apparatus.**

PSA performance was determined in terms of product purity and recovery following attainment of cyclic steady state. The fractional recovery was defined as the ratio of the number of net moles of nitrogen produced to the number of moles of nitrogen fed to the system. Both quantities were measured over several cycles via a wet test meter.

## Results and Discussion

Eleven operating variables were examined in PSA experiments. In each study, only the examined variable was changed and other variables were kept as constant as possible. About 24 hours of operation were required to reach cyclic steady state in each experiment because of transient effects in the product tank. All experimental conditions and corresponding results are summarized in Table 1.

The detailed results are discussed in the following sections. Prior to reviewing those, however, some general observations regarding comparisons of the experimental results and corresponding theoretical predictions are in order. For example, the most significant discrepancies between theory and experiment occur at either moderate pressure (e.g., 358 kPa) and low product purity, or high pressure (e.g., 620 kPa). Under those conditions, the assumptions of linearity and independence of the isotherms begin to break down. The former is evident in Figure 1, while the latter has been demonstrated by Miller et al. (1987) for oxygen in air with zeolite 5A at 25°C. Specifically, they found that, at oxygen partial pressures greater than about 0.5 bar, the mixed gas and pure component isotherms begin to deviate significantly. In PSA operation such high partial pressures are associated with low product purity and/or high total pressure during the feed step.

Another assumption that may have caused part of the discrepancy at moderate to high pressures is the presumption of Fickian diffusion and a constant diffusivity to represent the sorption mechanism within a particle. In diffusion through a porous solid, both bulk diffusion and Knudsen diffusion may contribute to the observed rate. As a limiting case when diffusion occurs in the Knudsen regime (i.e., at low pressures and in small pores), pressure does not affect the diffusivity; hence, that effect may be omitted as was done here. Conversely, since the molecular sieve particles are comprised of 1- to 10-$\mu$m-sized crystals and inert binder, the particles have a bidisperse pore size distribution. Thus, depending on conditions, diffusion may occur in the transition regime, and so the pressure effect on diffusivity may be significant.

For all that, the predicted and observed trends of performance are in good overall agreement: no significant systematic deviations are apparent. On the other hand, there exist some significant discrepancies between experimental and predicted performance in certain cases. Nevertheless, the average absolute differences between the experimental and predicted recoveries and product purities are only 2.52 and 1.81%, respectively.

### *Effect of duration and inlet velocity of high-pressure feed step*

The role of the high-pressure feed step is to produce the purified product. Since the concentration profile formed during high-pressure feed step is diffuse, increasing the amount of feed admitted results in lower purity product but a larger quantity of product. Even though more feed is consumed resulting in lower purity of the product and both of these effects tend to decrease recovery, the product recovery actually increases because the increase rate of the net amount of product is greater than those two opposing effects, Figures 3 and 4. The trade-off between product purity and recovery is a characteristic of diffusion-induced separation and is contrary to some ranges of equilibrium-based separations. This tendency is also exhibited in the following experimental results.

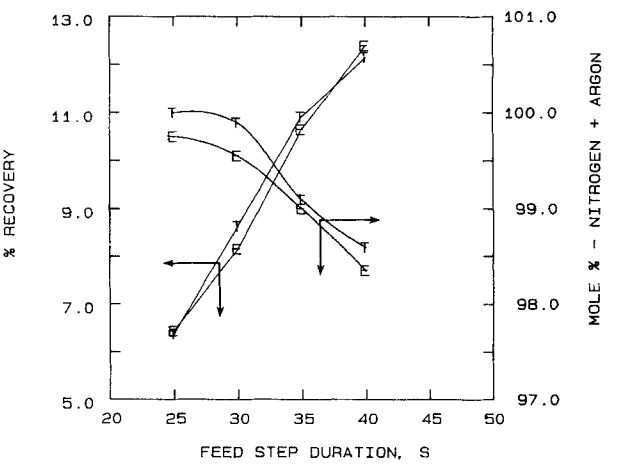


**Figure 3. Effect of feed step duration on product recovery and purity.**

*E* = experiment; *T* = theory. (See experiments 1–4 in Table 1 for conditions.)

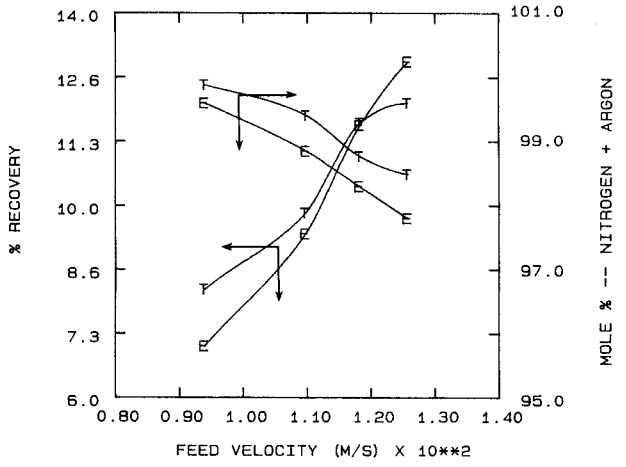


**Figure 4. Effect of feed velocity on product recovery and purity.**

*E* – experiment; *T* – theory. (See experiments 5–8 in Table 1 for conditions.)

To this point, the separate effects of increasing the amount of feed by increasing either the step duration or feed velocity have been discussed. Since they may be coupled phenomena, a subsequent series of experiments investigated the effect of the duration of the high-pressure feed step for a fixed amount of feed. Figure 5 shows how the feed velocity was changed to give the same number of moles of feed for each duration of that step. As shown in Figure 5, a short duration of the high-pressure step (for a fixed amount of feed) results in a small increase in product recovery, with no noticeable change in purity. On the other hand, at longer durations there is no significant change in product purity or recovery. The shorter duration apparently results in more product due to less adsorption of feed, but the product purity diminishes slightly because of the diffuse concentration profile formed during high-pressure feed step. Conversely, for a longer duration there is not much variation in product purity or recovery because adsorption approaches equilibrium more closely.

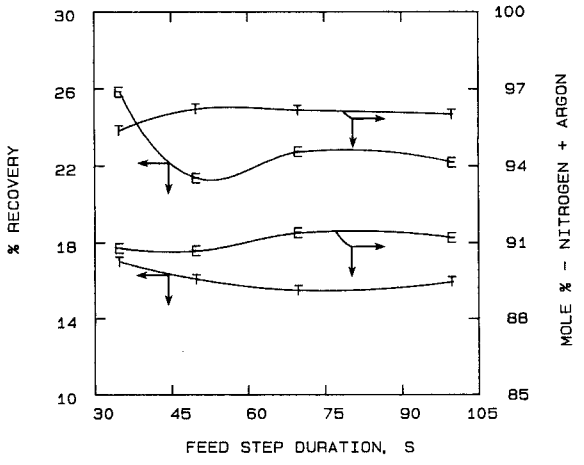


**Figure 5. Comparison of a short high pressure feed step with a long high pressure feed step for a fixed amount of feed.**

*E* – experiment; *T* – theory. (See experiments 9–12 in Table 1 for conditions.)

### *Effect of duration of the blowdown step*

Since a longer blowdown step allows more desorption of the adsorbed impurity oxygen, the capacity for the adsorption of oxygen will increase during the subsequent pressurization and high-pressure feed steps. In addition, the adsorbed nitrogen, which is the desired component, diffuses slowly out of the adsorbent during blowdown due to its lower diffusivity, which helps to cleanse the bed. Both of these effects result in purer product. Larger quantities of feed are required, however, during the pressurization step, and smaller quantities of net product are produced due to increased loss of gases as blowdown time increases. As a result, the recovery decreases, Figure 6. One more interesting point in this figure is that the product purity reaches a plateau for blowdown times greater than 10 s. Beyond 10 s, only the product recovery decreases without any significant increase in product purity. Therefore, the blowdown time should be determined with regard to this constraint.

### *Effect of the purge step velocity and duration*

The function of the purge step is to cleanse the bed by purging the column with part of the product stream produced during the high-pressure feed step. The bed can be more completely cleansed by simply using more purge gas. In Figure 7, the amount of purge gas is increased by increasing the purge gas velocity at constant duration. The results show that, even though there is a slight increase in product purity for higher purge velocity, the product recovery decreases drastically. In this set of experiments, the durations of the blowdown and purge step were 6 and 3 s, respectively. This means that 9 s of blowdown and purge was sufficient to remove much of the adsorbed oxygen and to allow cleansing action by desorbed nitrogen. Therefore, increasing the amount purged by simply increasing the purge gas velocity results only in a drastic decrease in recovery, without a significant concomitant increase in product purity.

Another way to increase the amount of purge gas is to increase the duration of the purge step, Figure 8. For those trials, the duration of the blowdown step was 2 s, and the duration of the purge step was varied from 3 to 11 s. The results show that, in the region of short purge time (less than 7 s), there is little increase in product purity. This small increase is probably due to greater desorption of oxygen and the self-cleansing effect

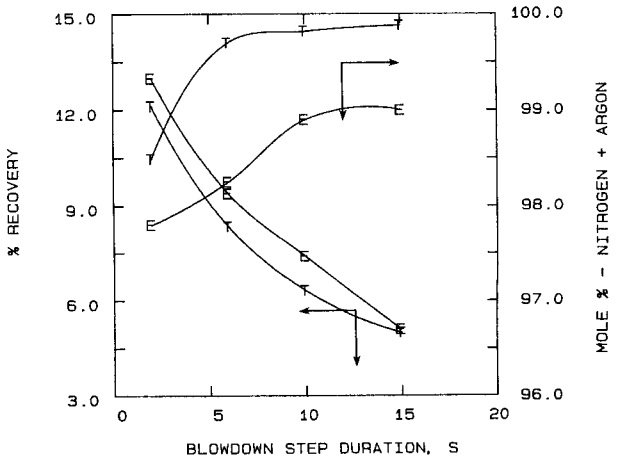


**Figure 6. Effect of blowdown step duration.**

*E* – experiment; *T* – theory. (See experiments 8 and 13–15 in Table 1 for conditions.)

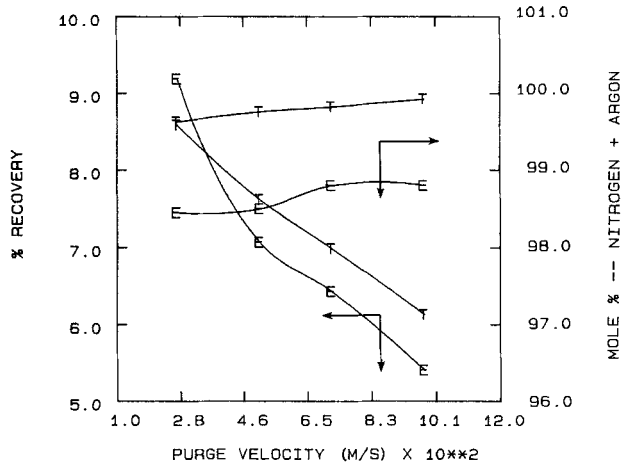


**Figure 7. Effect of purge velocity on product recovery and purity.**

*E* = experiment; *T* = theory. (See experiments 16–19 in Table 1 for conditions.)

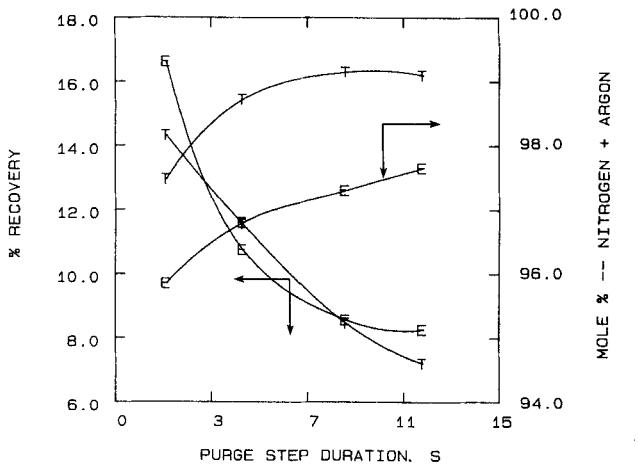


**Figure 9. Comparison of a short purge time with a long purge time for a fixed amount of purge gas.**

*E* = experiment; *T* = theory. (See experiments 24–27 in Table 1 for conditions.)

of gradual desorption of nitrogen, which does not occur during the blowdown step because of its short duration. At longer purge times, the purity reaches a plateau (similar to that observed in the results of the blowdown duration study), while the recovery drops drastically. The drop of recovery in this case is due to the combined effect of using more purge gas and increased desorption of gases. The results of Figures 7 and 8 indicate that using much purge gas to cleanse the bed tends to reduce recovery substantially.

The final parametric study of the purge step examined the effect of purge step duration for a fixed amount of purge gas. The purge velocity is varied according to the duration to give the same number of moles of purge gas, Figure 9. The results show that, as the duration increases, the purity increases gradually, but the recovery decreases drastically. This trend is expected because the longer duration of the purge step allows increased desorption of gases and thus results in lower recovery but purer product. The more significant increase of purity in Figure 9, as compared to the previous results, is due to the use of a higher inlet velocity during the high-pressure feed step in this set of experiments.

### *Effect of duration of the pressurization step*

The effects of the duration of the pressurization step at cyclic steady state are given in Figure 10. The results show that, as the duration increases, the purity decreases but the recovery increases. Since nitrogen is the more strongly adsorbed component, longer duration permits greater adsorption of nitrogen. In contrast, oxygen is taken up (to the equilibrium limit) nearly instantaneously. So, as the time allowed for pressurization increases, the gas phase becomes proportionately richer in oxygen and the subsequent product purity decreases. Also, since more gas is adsorbed as the pressurization step is prolonged, additional adsorption of gases during high-pressure feed step is prevented, and more product is produced, though at low purity. The consumption of more feed, due to longer pressurization and the resulting lower product purity, contributes to a decrease in recovery. The product quantity, however, increases at an even

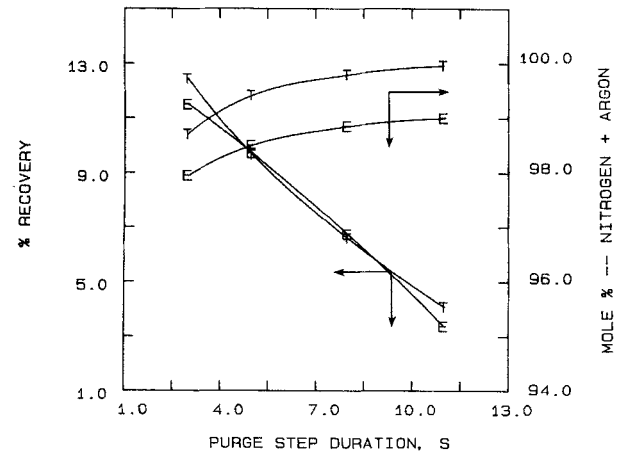


**Figure 8. Effect of purge step duration on product recovery and purity.**

*E* = experiment; *T* = theory. (See experiments 20–23 in Table 1 for conditions.)

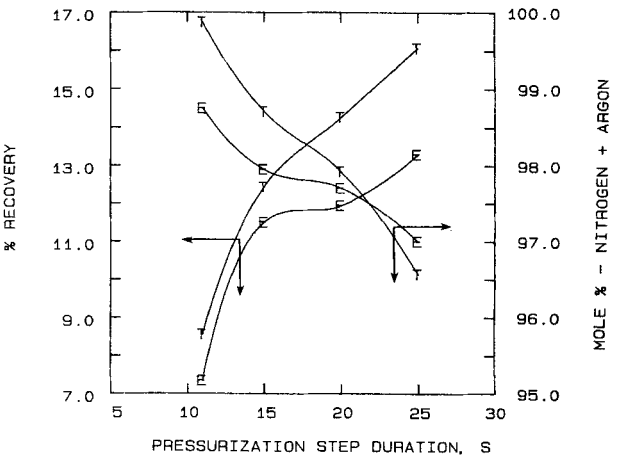


**Figure 10. Effect of pressurization step duration.**

*E* = experiment; *T* = theory. (See experiments 20 and 28–30 in Table 1 for conditions.)

Table 3. Effect of Pressure Ratio*

| Expt. No. | Pres. Ratio | % Recovery | $N_2$ mol % | Productivity Ratio |
|---|---|---|---|---|
| 31 | 1.755 | 41.56 | 82.3 | 4.78 |
| 32 | 2.909 | 22.46 | 93.7 | 3.90 |
| 33 | 4.039 | 12.54 | 98.2 | 2.61 |
| 34 | 1.763 | 13.83 | 93.8 | 1 |
| 32 | 2.909 | 22.46 | 93.7 | 3.90 |
| 35 | 4.074 | 23.05 | 93.7 | 5.46 |

*Standard conditions: $t_1 = 35$ s; $t_2 = 2$ s; $t_3 = 3$ s; $t_4 = 15$ s; $N_{Pu} = 0.0166 \times 10^{-3}$ m$^3$ at STP.

greater rate and offsets these two effects. Thus, the overall effect is that recovery increases for longer pressurization times.

### *Effect of the pressure ratio*

The effect of the pressure ratio was studied by changing the high pressure while the low pressure was kept nearly constant, Table 3. The first three results, which were obtained by keeping constant all parameters except for pressure ratio, show that as the pressure ratio increases the purity increases but the recovery decreases. The diverging trends make comparison of the three pressure ratios unclear. So, another set of PSA experiments was performed to obtain the same purity for three different pressure ratios, i.e., by adjusting the inlet velocity during high-pressure feed step. The results are given in the last three entries in Table 3. Even though there is a large increase in recovery in the low-pressure-ratio region, that effect diminishes at higher pressure ratios. Despite that, the productivity increases consistently as the pressure ratio increases. The small recovery increase at high pressure ratios is partly due to the rate of increase in the total amount of feed being greater than that of the net product.

### *Effect of subatmospheric blowdown and purge*

The removal of oxygen can be facilitated by applying vacuum to a bed during blowdown and purge step. By doing so, purer product is obtained, but recovery decreases due to greater desorption of nitrogen as compared with atmospheric blowdown and purge, Table 4. For a direct comparison, the same purity of product was obtained by adjusting the feed velocity (in the same manner as discussed in the previous section). As shown in Table 5, subatmospheric blowdown and purge are advantageous at low feed pressures, but the advantage disappears as feed pressure increases. This effect may have been caused by the reduction of the time necessary for blowdown when the feed pressure was low. That enhanced the removal of oxygen from the bed, which improved performance. Nevertheless, at higher feed pressures, atmospheric blowdown and purge are sufficient to remove oxygen.

### *Effect of column geometry*

To study the effect of column geometry, three columns of varying $L/d$ but constant volume were used in PSA experiments, Tables 1, 2 and 6. The same duration of each step and the same amount of feed and purge were used, so the only variation was due to the shape differences. Table 6 shows that the column having lowest $L/d$ gives poorest performance in product purity as well as recovery. This trend was explained by the theoretical model in our previous paper. Lower interstitial velocities, due to larger column diameters (and shortened column lengths), result in a decrease in the Peclet number. There is a slight compensation due to the slight decrease in the axial dispersion coefficient due to the lower interstitial velocity, which contributes to an increase in the Peclet number. It is expected that the decrease in Peclet number results in poorer separation. In actual experiments, channeling and/or maldistribution of influent and effluent in fatter columns might also have caused poorer separation.

## Conclusions

Nitrogen separation from air has been successfully performed with molecular sieve RS-10 by using four-step PSA cycle. Systematic studies of important PSA operating parameters included step times, feed and purge velocities, pressure ratio, subatmospheric blowdown and purge, and column geometry. The results may provide guidance for determining operating policies of actual PSA systems.

Trade-offs between recovery and purity were observed for many operating variables, as were interactions among the vari-

Table 4. Blowdown and Purge for Idential Conditions: Atmospheric vs. Subatmospheric*

| | 200 kPa | | 358 kPa | | 620 kPa | |
|---|---|---|---|---|---|---|
| High Pres. | Atmospheric | Substmospheric | Atmospheric | Subatmospheric | Atmospheric | Subatmospheric |
| Expt. No. | 31 | 36 | 32 | 37 | 33 | 38 |
| % Recovery | 41.56 | 28.89 | 22.46 | 19.05 | 12.54 | 12.03 |
| $N_2$, mol % | 82.30 | 86.15 | 93.70 | 95.05 | 98.20 | 98.40 |

*Standard conditions: $t_1 = 35$ s; $t_2 = 2$ s; $t_3 = 3$ s; $t_4 = 15$ s; $N_H = 0.393 \times 10^{-3}$ m$^3$ at STP; $N_{Pu} = 0.0166 \times 10^{-3}$ m$^3$ at STP.

Table 5. Blowdown and Purge for the Same Products Purity: Atmospheric vs. Subatmospheric*

| | 200 kPa | | 358 kPa | | 620 kPa | |
|---|---|---|---|---|---|---|
| High Pres. | Atmospheric | Substmospheric | Atmospheric | Subatmospheric | Atmospheric | Subatmospheric |
| Expt. No. | 34 | 39 | 32 | 40 | 35 | 41 |
| % Recovery | 13.83 | 16.87 | 22.46 | 21.83 | 23.05 | 23.12 |
| $N_2$, mol % | 93.8 | 93.8 | 93.7 | 93.7 | 93.7 | 93.7 |

*Standard conditions: $t_1 = 35$ s; $t_2 = 2$ s; $t_3 = 3$ s; $t_4 = 15$ s; $N_{Pu} = 0.0166 \times 10^{-3}$ m$^3$ at STP.

**Table 6. Effect of Column Geometry**

| Column | I | II | III |
|---|---|---|---|
| Expt. No. | 9 | 42 | 43 |
| % Recovery | 25.84 | 22.40 | 22.37 |
| $N_2$, mol % | 90.8 | 89.0 | 82.3 |
| Column Dimensions | | | |
| I: $d = 0.0208$ m | $L = 1.016$ m | | |
| II: $d = 0.0394$ m | $L = 0.284$ m | | |
| III: $d = 0.0635$ m | $L = 0.109$ m | | |
| Standard Conditions | | | |
| $t_1 = 35$ s | $t_2 = 2$ s | | |
| $t_3 = 3$ s | $t_4 = 15$ s | | |
| $N_H = 0.393 \times 10^{-3}$ m$^3$ at STP | $N_{Pu} = 0.0166 \times 10^{-3}$ m$^3$ at STP | | |

ables. Those trade-offs and interactions, which for certain combinations proved to be contrary to intuition, made it difficult to predict PSA performance by simple generalized rules. Therefore, numerical simulation, along with some degree of experimental verification, is practically essential for achieving a thorough understanding of diffusion-induced PSA performance.

Theoretical results were obtained by numerical simulation with a fairly simple model. Only two parameters were determined empirically, *viz.*, the effective diffusivity of oxygen and the effective diffusivity ratio of nitrogen and oxygen. The values obtained were $3.0 \times 10^{-7}$ m$^2$/s and 0.02, respectively. These values were not varied subsequently, and the predicted trends were found to be in close agreement with those of experiments at 43 sets of conditions by varying 11 operating conditions or design parameters. In fact, the average absolute differences between experimental and predicted recoveries and product purities were only 2.52 and 1.81%, respectively. These errors seem relatively small in view of the ranges of the variables studied and the inherent complexity of the process.

## Acknowledgments

This research was partially sponsored by the U.S. Air Force Office of Scientific Research/AFSC, under contract. The support of K. G. Ikels of the School of Aerospace Medicine, Brooks AFB, Texas, is gratefully acknowledged. The instruments were provided, in part, by funds from NSF Grant Number CPE-8405892. Finally, the supply of molecular sieve by Union Carbide Corp. is acknowledged.

## Literature Cited

Ball, D. J., "Comparison of the Static and Dynamic Sorption Capacities of 4A and 5A Zeolites," M.S. Thesis, Ohio State Univ. (1985).

Edwards, M. F., and J. F. Richardson, "Gas Dispersion in Packed Bed," *Chem. Eng. Sci.*, **23,** 109 (1968).

Doong, S. J., and R. T. Yang, "Bulk Separation of Multicomponent Gas Mixture by Pressure Swing Adsorption: Pore/Surface Diffusion and Equilibrium Models," *AIChE J.*, **32,** 397 (1986).

———, "Bidisperse Pore Diffusion Model for Zeolite Pressure Swing Adsorption," *AIChE J.*, **33,** 1045 (1987).

Hassan, M. M., N. S. Raghavan, and D. M. Ruthven, "Pressure Swing Air Separation on a Carbon Molecular Sieve: II. Investigation of a Modified Cycle with Pressure Equalization and No Purge," *Chem. Eng. Sci.*, **27,** 2037 (1987).

———, "Air Separation by Pressure Swing Adsorption on a Carbon Molecular Sieve," *Chem. Eng. Sci.*, **41,** 1333 (1986).

Miller, G. W., K. S. Knaebel, and K. G. Ikels, "Equilibria of Nitrogen, Oxygen, Argon, and Air in Molecular Sieve 5A," *AIChE J.*, **33,** 194 (1987).

Ruthven, D. M., *Principles of Adsorption and Adsorption Processes.* Wiley, New York (1984).

Shin, H. S., and K. S. Knaebel, "Pressure Swing Adsorption: A Theoretical Study of Diffusion-Induced Separations," *AIChE J.*, **33,** 654 (1987).

Wankat, P. C., *Large-Scale Adsorption and Chromatography,* **II,** CRC Press, Boca Raton, FL (1986).

Yang, R. T., *Gas Separation by Adsorption Processes,* Butterworths, Stoneham, MA (1987).

Yang, R. T., and S. J. Doong, "Gas Separation by Pressure Swing Adsorption: A Pore-Diffusion Model for Bulk Separation," *AIChE J.*, **31,** 1829 (1985).

*Manuscript received March 1, 1988, and revision received May 16, 1988.*

## Notation

$d$ = column inner diameter
$L$ = column length
$N$ = volume at STP of gas entering column during step indicated by subscript, $H$ or $Pu$
$t_j$ = duration of step $j$

### *Subscripts*

$H$ = high-pressure feed step
$j$ = step $j$, 1 to 4
$Pu$ = purge step
1 = high-pressure feed step
2 = blowdown step
3 = purge step
4 = pressurization step